

High-precision broadband linear polarimetry of early-type binaries III. AO Cassiopeiae revisited^{*}

Yasir Abdul Qadir¹, Andrei V. Berdyugin¹, Vilppu Piirola¹,
Takeshi Sakanoi², and Masato Kagitani²

¹ Department of Physics and Astronomy, FI-20014 University of Turku, Finland
e-mail: yasir.abdulqadir@utu.fi

² Graduate School of Sciences, Tohoku University, Aoba-ku, 980-8578 Sendai, Japan

Received 12 November 2022 / Accepted 17 January 2023

ABSTRACT

Aims. The fact that the O-type close binary star system AO Cassiopeiae exhibits variable phase-locked linear polarization has been known since the mid-1970s. In this work, we re-observe the polarization arising from this system more than 50 years later to better estimate the interstellar polarization and to independently derive the orbital parameters, such as inclination, i , orientation, Ω , and the direction of the rotation for the inner orbit from the phase-folded polarization curves of the Stokes q and u parameters.

Methods. The Dipol-2 polarimeter was used to obtain linear polarization measurements of AO Cassiopeiae in the B , V , and R passbands with the T60 remotely controlled telescope at an unprecedented accuracy level of $\sim 0.003\%$. We have obtained the first proper quantification of the interstellar polarization in the direction heading towards AO Cas by observing the polarization of three neighboring field stars. We employed a Lomb-Scargle algorithm and detected a clear periodic signal for the orbital period of AO Cas. The standard analytical method based on a two-harmonics Fourier fit was used to obtain the inclination and orientation of the binary orbit.

Results. Our polarimetric data exhibited an unambiguous periodic signal at 1.76 days, thus confirming the orbital period of the binary system of 3.52 days. Most of the observed polarization is of interstellar origin. The de-biased values of the orbital inclination are $i = 63^\circ + 2^\circ / - 3^\circ$ and orientation of $\Omega = 29^\circ(209^\circ) \pm 8^\circ$. The direction of the binary system rotation on the plane of the sky is clockwise.

Key words. polarization – techniques: polarimetric – instrumentation: polarimeters – stars: individual: AO Cassiopeiae – binaries (including multiple): close – binaries: eclipsing

1. Introduction

AO Cassiopeiae (AO Cas) is an early-type binary system that consists of a larger, but less massive O9-III primary and late O-type main sequence secondary, with an orbital period of about 3.5 days and a mass ratio of $q = M_s/M_p = 1.47 \pm 0.08$ (Gies & Wiggs 1991). The AO Cas light curve exhibits only grazing eclipses and most of the light variations are due to geometrical distortion of the primary component. Apparently, the primary star fills its Roche lobe (Hutchings & Hill 1971), or is close to filling it (Gies & Wiggs 1991), and the system is likely to be engaged in a slow mass-exchange stage (Plavec 1970). There is a clear spectroscopic evidence for the presence of high-density gas in the system and the behavior of the H_α profile indicates the existence of the ionized bow shock area where the stellar winds collide (Gies & Wiggs 1991).

Because of its brightness, AO Cas has been an early target for polarimetric observations. The first attempt to observe polarization from this binary system was made by Shakhovskoj (1964), who came to the conclusion that AO Cas did not exhibit any variable polarization. This was due to the fact that the

observational errors were rather large $\sim 0.09\%$ and no filters were used to conduct those observations.

The first successful variable polarimetric signals synchronous with the orbital phase from AO Cas were detected and reported by Pfeiffer & Koch (1973a), Pfeiffer & Koch (1973b), and Pfeiffer & Koch (1976). It was then proposed by Pfeiffer (1976) that the variable phase-locked polarization arises from scattering material within a large circumstellar envelope. The observed polarization is altered at times by events related to the mass exchange process within the binary system. It was further suggested that this large circumstellar envelope contains most of the scattering material, which is highly ionized. A suggestion was made to continue observing the system in order to track any changes that could occur in the observed polarization of the system (Pfeiffer 1976).

A substantially better polarization data set for AO Cas, in terms of in quality and accuracy, has been obtained by Rudy & Kemp (1976). Their data analysis led to the conclusion that polarization arises from the light scattering on the gaseous stream, with the main contribution to polarization coming from the relatively small region located on the advancing side of the secondary star Rudy & Kemp (1976). Later, these data were re-used by Rudy & Kemp (1978), Brown et al. (1978), Simmons et al. (1982) and Aspin & Simmons (1982) for estimations of the orbital inclination as well as in discussions of the accuracy of the orbit inclinations derived for the binary

^{*} The polarization data for AO Cas are only available in electronic form at the CDS via anonymous ftp to cdsarc.cds.unistra.fr (130.79.128.5) or via <https://cdsarc.cds.unistra.fr/cgi-bin/qcat?J/A+A/>

systems from polarization data. No definite conclusions on the exact location of the light-scattering region have been made and the apparent controversy between two different interpretations remains unresolved.

Since the 1970s, AO Cas system has never been observed polarimetrically. Thus, the question about the apparent seasonal variations of intrinsic polarization raised by (Pfeiffer 1976) remained unaddressed. There has been a level of uncertainty around the amount of interstellar (IS) component in the observed polarization of AO Cas because two estimates of this polarization, obtained by Pfeiffer (1976) and Brown et al. (1978), differ dramatically. Therefore, we have decided to this binary system to study the polarization variability in more detail, determine the amount of interstellar polarization with a good level of confidence, and compare new polarization measurements with the previous ones. In this paper, describe the results of our new high-precision, three-band *BVR* polarimetry of AO Cas.

2. Polarimetric observations

2.1. DiPol-2

We observed AO Cas for a total of 39 nights, from October 26, 2020 until February 01, 2021, with the DiPol-2 polarimeter (Piirola et al. 2014), attached to the remotely controlled T60 telescope at Haleakalā Observatory, Hawaii. The observational log is given in Table A.1.

DiPol-2 uses two dichroic beam-splitters that split the incident light beam into the *B*, *V*, and *R* passbands, which are simultaneously recorded by three CCD cameras. The polarization modulator is a rotatable superachromatic $\lambda/2$ (or $\lambda/4$) plate and the polarization analyzer is a plane-parallel calcite plate. A typical cycle of linear polarimetric measurement consists of 16 exposures at the orientation intervals of 22.5° of the $\lambda/2$ plate. The calcite plate produces two orthogonally polarized stellar images that are recorded simultaneously to eliminate errors that may arise due to varying atmospheric transparency; thus, the contribution from the sky polarization is automatically canceled out.

For observations of the bright stars, such as AO Cas, DiPol-2 employs the intentional defocusing technique, whereby the stellar image is spread over the large number of pixels. This allows us to collect up to 10^7 photo-electrons per exposure and avoid pixel saturation. Generally, around 180 – 320 images were taken every night with the exposure time of 3s. This corresponds to 45 – 80 measurements of Stokes q and u per night. The skyflat images that are used for calibration purposes were regularly taken at twilight hours, either in the beginning of the observing night or at dawn. Once per night, the series of dark and bias images were also taken.

The telescope polarization was derived from observations of 20–25 zero-polarized standard stars. It was found to be in the range between 0.004% – 0.006%. The accuracy of the determination of instrumental polarization is 0.0002% – 0.0003%. Polarization values for AO Cas have been corrected for instrumental polarization. For the calibration of polarization angle zero-point, polarization angles of highly polarized (5% – 6%) standard stars HD 204827 and HD 25443 were used. Their polarization angles are given in Table 1.

The resulting accuracy in the case of AO Cas is at the level of 0.002% – 0.003% in the *B* passband and 0.003% – 0.005% in the *V* and *R* passbands. Thus, our accuracy is on an order of

Table 1. Average polarization angles (θ) of highly polarized stars.

Star	Passband	θ [deg]	References
HD 204827	<i>B</i>	57.79 ± 0.02	[1]
	<i>V</i>	58.33 ± 0.02	[1]
	<i>R</i>	59.21 ± 0.02	[1]
HD 25443	<i>B</i>	134.28 ± 0.51	[2]
	<i>V</i>	134.23 ± 0.34	[2]
	<i>R</i>	133.65 ± 0.28	[2]

References. (1) Piirola et al. (2021); (2) Schmidt et al. (1992).

magnitude that is higher than the value $\sigma_p \sim 0.025\%$ that was previously obtained by Rudy & Kemp (1976).

2.2. Data reduction

The subtraction of bias and dark frames and the application of flat-fielding in order to eliminate any spurious effects arising from these imperfections was performed via automated Visual Basic scripts that are capable of processing several hundreds of polarimetry CCD images simultaneously. A special algorithm has been developed to pre-align images taken in long series of polarimetric sequences to remove possible effect of the image drift. The scripts, executed with the Maxim DL Pro¹, perform the calibration and create 2 x 2 binned sub-frames for every taken raw image.

Normalized Stokes parameters q and u are computed from the flux intensity ratios of the orthogonally polarized stellar images $Q_i = I_e(i)/I_o(i)$ obtained for each orientation of wave plate, $i = 0.0^\circ, 22.5^\circ, 45.0^\circ, 67.5^\circ$, as:

$$\begin{aligned} Q_m &= Q_{0.0} + Q_{22.5} + Q_{45.0} + Q_{67.5}, \\ q &= (Q_{0.0} - Q_{45.0})/Q_m, \\ u &= (Q_{22.5} - Q_{67.5})/Q_m. \end{aligned} \quad (1)$$

Because AO Cas is a bright target, intentional defocusing was used (see Piirola et al. (2014) and Piirola et al. (2021)). Typical software aperture size for the defocused stellar image was chosen as $\sim 7 - 10$ arcsec. This allows us to collect up to 10^7 ADUs per image, avoiding image saturation while keeping the o and e-images well separated (and not overlaid). The distance between the centers of o and e-images in the focal plane is ~ 22 arcsec. The intensities $I_e(i)$ and $I_o(i)$ were determined from the series of calibrated polarimetry images with the aperture photometry method implemented as a standard feature in the Maxim DL Pro software. A simple FORTRAN code was used to compute the Stokes parameters q and u from each set of four images. This code also computes weighted average values of polarization. It gives lower weight to individual measurements of Stokes q and u that deviate from the mean value by more than expected from Gaussian noise distribution. All the measurement points that were within 2σ were given an equal weight and any points that deviated more 2σ were given a lower weight that was proportional to the inverse square of the estimated error. Any points beyond 3σ were rejected. Using Stokes parameters q and u , the code computes the values of polarization P and polarization angle θ .

¹ <https://diffractionlimited.com/downloads/GettingStarted.pdf>

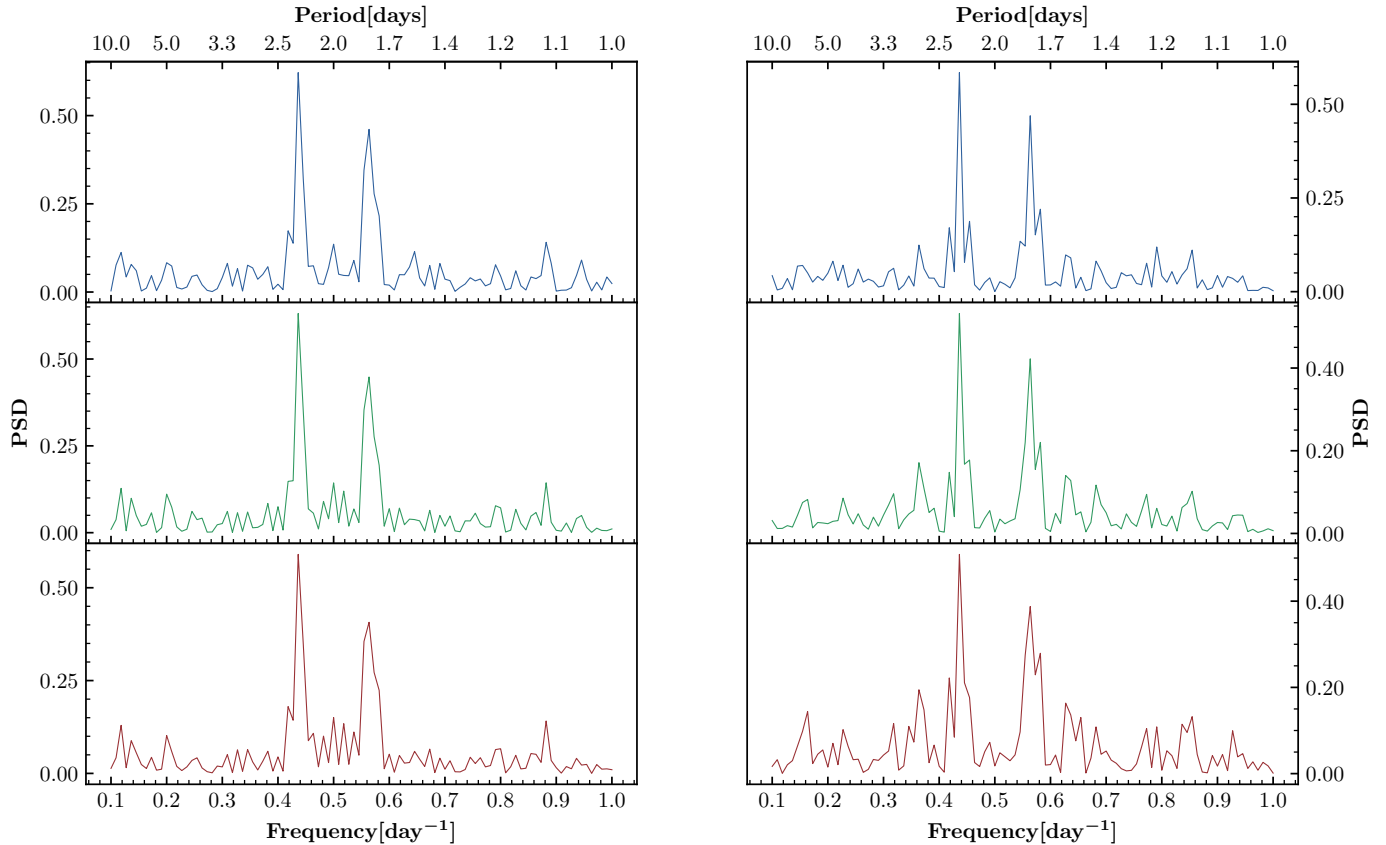


Fig. 1. Lomb-Scargle periodograms for Stokes q (left column) and u (right column) of AO Cas in B , V , and R passbands (top, middle and bottom panels respectively).

Table 2. FAP for AO Cas Periodograms.

	Passband	Period [days]	FAP
Stokes q :	B	1.76	1.84×10^{-10}
		2.31	1.75×10^{-9}
	V	1.76	5.7×10^{-11}
		2.31	2.88×10^{-10}
	R	1.76	1.67×10^{-10}
		2.31	1.16×10^{-9}
Stokes u :	B	1.76	9.5×10^{-11}
		2.31	8.0×10^{-9}
	V	1.76	1.28×10^{-8}
		2.31	1.01×10^{-7}
	R	1.76	6.95×10^{-8}
		2.31	2.78×10^{-6}

3. Data analysis

3.1. Period search

After re-observing AO Cas polarimetrically after a time span of more than 50 years, we decided to perform a rigorous period search utilizing our new high-precision polarization data. We employed a Lomb-Scargle algorithm (Lomb 1976; Scargle 1982) from `astropy.timeseries`² (Price-Whelan et al. 2018) in PYTHON to determine any periodic signals which may present in polarimetric data. The advantage in using Lomb-Scargle

² <https://docs.astropy.org/en/stable/timeseries/lombscargle.html>

periodogram is that the algorithm utilizes a least-squares method to fit a sinusoidal on unevenly sampled data (which it is often the case with respect to astronomical data).

Due to the orbital motion, the degree of intrinsic polarization from the scattered light in a binary system usually reaches maximum when the scattering angle is near 90° or 270° and minimum when it is near 0° or 180° . Therefore, Lomb-Scargle periodograms applied to polarization data is expected to detect only half of the orbital period for systems such as AO Cas. To visualize the periodic search in our data, we plotted Lomb-Scargle periodograms for both Stokes q and u in B , V , and R passbands (Figure 1). All these periodograms show two very prominent peaks: 1) at 1.76 days, namely, half of the known orbital period of AO Cas; and 2) the nearby peak at 2.31 days.

We believe that the peak seen at 2.31 days is nothing but an alias peak of the main peak at 1.76 days. The alias peaks can be produced by periodicity in the timing of observations coupled with the periodic nature of the source that is being observed. If that period is not less than half of the sampling frequency, that is, the Nyquist frequency (f_{ny}), then there is a side effect that produces two waves that differ by $1/f_{\text{ny}}$. With the (half) orbital period for AO Cas, ~ 1.76 days, which corresponds to the frequency of 0.57; this is more than half of the sampling frequency of ~ 0.4 , as we used data from 39 nights that were observed over a period of about 100 days. Therefore, an alias peak can be expected at $1/(1-1/1.76) = 2.31$ days, which is exactly where the periodograms show the alias peaks (cf. Shannon (1949); VanderPlas (2018)). A similar phenomenon

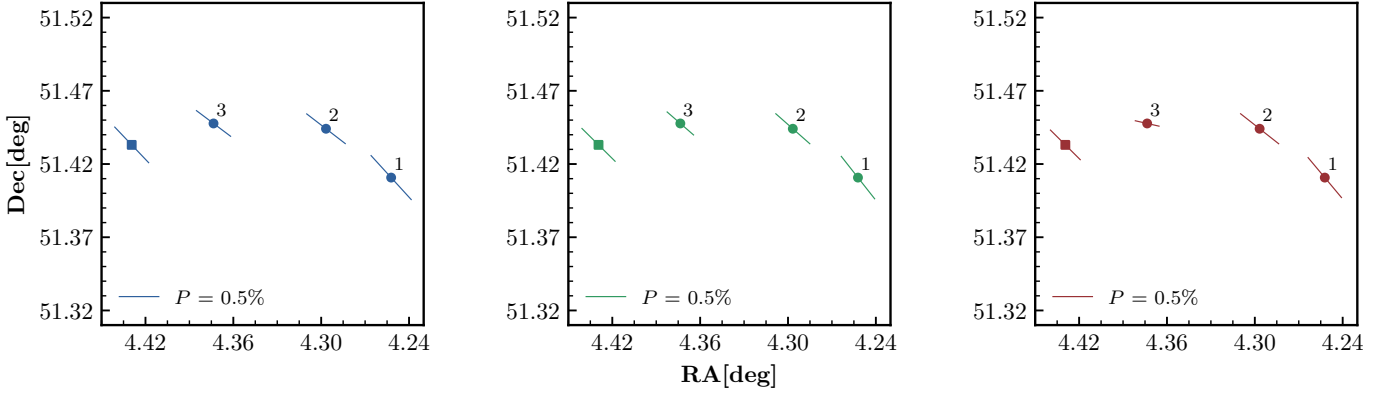


Fig. 2. Polarization map of AO Cas (square) and field stars (circles) in *B* (left panel), *V* (middle panel), and *R* (right panel) passbands. The length of the bars corresponds to the degree of observed polarization P , and the direction corresponds to the polarization angle (measured from the north to the east). The field stars are numbered the same as in Table 3.

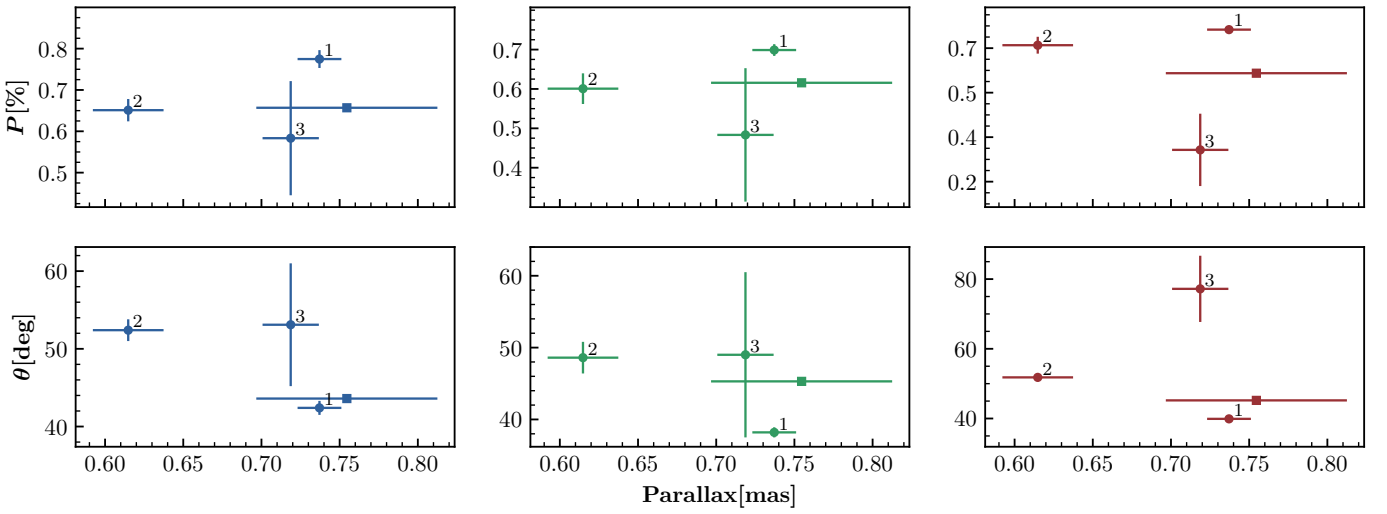


Fig. 3. Dependence of the observed degree of polarization P (top panels) and polarization angle θ (bottom panels) in *B* (left panels), *V* (middle panels), and *R* (right panels) passbands on parallax of AO Cas (square) and field stars (circles) with reference numbers that are same as in Table 3. The error bars correspond to $\pm\sigma$ errors.

Table 3. Identifiers, coordinates, parallaxes, Stokes parameters, polarization degrees and angles, and number of exposures for each field star.

Identifier [Gaia DR3]	Coordinates [J2000d]	Parallax [mas]	Passband	Stokes q [%]	Stokes u [%]	P [%]	error ^a [%]	θ [deg]	N_{exp}
395017526722293248 (Ref 1)	4.252220267, 51.41073703	0.7371 ± 0.014	<i>B</i>	0.073	0.809	0.812	0.026	42.4 ± 0.9	320
			<i>V</i>	0.174	0.715	0.736	0.018	38.2 ± 0.7	320
			<i>R</i>	0.125	0.699	0.710	0.009	39.9 ± 0.4	320
395017801600190336 (Ref 2)	4.29671658, 51.44408771	0.6148 ± 0.023	<i>B</i>	-0.169	0.642	0.664	0.032	52.4 ± 1.4	128
			<i>V</i>	-0.078	0.613	0.618	0.047	48.6 ± 2.2	128
			<i>R</i>	-0.156	0.643	0.661	0.026	51.8 ± 1.1	128
394976810432321792 (Ref 3)	4.37352903, 51.44770379	0.7187 ± 0.018	<i>B</i>	-0.162	0.560	0.583	0.166	53.9 ± 7.9	64
			<i>V</i>	-0.066	0.473	0.478	0.203	49.0 ± 11.5	64
			<i>R</i>	-0.300	0.143	0.332	0.114	77.2 ± 9.5	64

Notes. ^(a) The error value is same for Stokes q , Stokes u , and P in each corresponding row.

was observed by Kosenkov & Veledina (2018) when deducing superhump period of the black hole X-ray binary GX 339–4.

Furthermore, we calculated the false alarm probability (FAP) by using a bootstrap method (Suveges 2012) for peaks associated with the orbital period of AO Cas as well as their alias peaks. These values are given in Table 2, which shows that

FAP for the peaks associated with the "polarimetric" orbital period is very low, but the same is true for alias peaks as well, since the algorithm cannot distinguish between the real peak and its alias peak. Since the orbital period of AO Cas is already known to be 3.5 days, we can conclude that the real peak is the one seen at 1.76 days. Therefore, it can be deduced that the

Table 4. Average observed P_{obs} , θ_{obs} , average interstellar P_{is} , θ_{is} , and average intrinsic P_{int} , θ_{int} of AO Cas.

Passband	P_{obs} [%]	θ_{obs} [deg]	P_{is} [%]	θ_{is} [deg]	P_{int} [%]	θ_{int} [deg]
<i>B</i>	0.671 ± 0.003	43.6 ± 0.1	0.741 ± 0.021	45.9 ± 0.8	0.091 ± 0.021	154.3 ± 0.1
<i>V</i>	0.636 ± 0.002	45.3 ± 0.1	0.714 ± 0.017	39.3 ± 0.7	0.161 ± 0.017	101.6 ± 0.1
<i>R</i>	0.573 ± 0.003	45.2 ± 0.1	0.698 ± 0.010	41.2 ± 0.4	0.153 ± 0.010	115.4 ± 0.1

period search algorithm applied to the new polarization data has clearly revealed the orbital period of the binary system. We have not detected any other periods in our polarization data of AO Cas.

3.2. Interstellar polarization

The observed polarization P_{obs} of almost every distant star contains not only the intrinsic polarization component, but also the interstellar (IS) polarization component, P_{is} , which is due to interstellar dust. Since the observed average polarization of AO Cas is rather high ($\sim 0.6\%$) and the distance to the binary is large (~ 1300 pc (Gaia Collaboration et al. 2021)), one can expect significant contribution of the P_{is} component. The IS polarization for AO Cas has been estimated by (Pfeiffer 1976) for the *B* and *V* passbands as $P_{\text{is}} = 1.2 \pm 0.2\%$, $\theta_{\text{is}} = 80^\circ \pm 5^\circ$. After subtraction of IS component, Pfeiffer got intrinsic polarization value for AO Cas peaking at $P_{\text{int}} \geq 1.5\%$, (cf. Figs. 2 and 3 from (Pfeiffer 1976)). Later on, (Brown et al. 1978) re-evaluated IS polarization component for AO Cas and got significantly smaller value of $P_{\text{is}} = 0.5\%$ with the direction $\theta_{\text{is}} = 55^\circ$.

In order to obtain more reliable estimates for the P_{is} and θ_{is} , we decided to conduct polarimetric observations of field stars in the close proximity of AO Cas. We used the GAIA database³ to search for stars within the angular distances of $\leq 7'$ from AO Cas and parallaxes between $0.6 - 0.8$ mas, as the parallax of AO Cas itself is 0.76 ± 0.06 mas (Gaia Collaboration et al. 2021). Three such stars have been found and observed.

In Figure 2, we have plotted the polarization maps that show the distribution of IS polarization vectors around AO Cas in *B*, *V*, and *R* passbands. Table 3 gives their Gaia identifiers, coordinates, parallaxes, Stokes parameters, polarization degrees and angles, and the total number of exposures. Figure 3 shows the dependence of field stars polarizations and polarization angles on the parallax. Using these data, we have calculated weighted mean values for the IS polarization. In Table 4, we are showing average observed polarization degree P_{obs} and angle θ_{obs} , the interstellar polarization degree P_{is} and angle θ_{is} , and the average intrinsic polarization degree, P_{int} and angle θ_{int} , together with their errors in each passband for AO Cas. We used the average of all nightly measurements for both AO Cas and field stars where we observed the data for more than one night.

As is seen from Table 4, the IS polarization degree derived by us, $P_{\text{is}} \sim 0.7\%$ is significantly lower than that derived by Pfeiffer, but larger than derived by (Brown et al. 1978). The new IS polarization angle, $\theta_{\text{is}} \sim 40^\circ$, is also different from both of the previously determined values. Given the new reliable estimates of the IS polarization parameters, it becomes obvious that most of the observed polarization in AO Cas is due to interstellar dust. The value of intrinsic polarization in this binary is rather small: $P_{\text{int}} \approx 0.1 - 0.2\%$. It appears that previous estimates for $P_{\text{int}} > 1.0\%$ made by (Pfeiffer 1976)

were based on wrong adopted parameters of the IS polarization component. Thus, the presence of a large circumstellar envelope, which would otherwise need to exist to produce such a large intrinsic polarization, can be ruled out.

3.3. Polarization variability

The common method of analysis of the phase-locked binary polarization is fitting the phase curves of the Stokes parameters q and u with Fourier series expansion. This method is also known as the "BME" approach, (Brown et al. 1978). For a circular orbit with co-rotating light scattering envelope, this fit includes only zeroth, first and second harmonics terms:

$$\begin{aligned} q &= q_0 + q_1 \cos \lambda + q_2 \sin \lambda + q_3 \cos 2\lambda + q_4 \sin 2\lambda, \\ u &= u_0 + u_1 \cos \lambda + u_2 \sin \lambda + u_3 \cos 2\lambda + u_4 \sin 2\lambda, \end{aligned} \quad (2)$$

where, $\lambda = 2\pi\phi$ and ϕ is a phase of the orbital period. We used `curve_fit` function of `scipy.optimize`⁴ library in PYTHON to obtain best fit parameters together with their errors. They are shown in Table 5. After deriving Fourier coefficients from the best fits to each passband, we plotted the fitted curves over the observational data points in Figure 4. The ephemeris which has been used is: P_{orb} [days] = 3.52348, T_0 [MJD] = 2445294.97083⁵. Phase 0.0 corresponds to the primary minimum.

It is possible to derive the orbital inclination i using the values of the first ($q_{1,2}$, $u_{1,2}$) and second ($q_{3,4}$, $u_{3,4}$) harmonics terms of Fourier series with the following formulas (Drissen et al. 1986):

$$\left(\frac{1 - \cos i}{1 + \cos i} \right)^4 = \frac{(u_1 + q_2)^2 + (u_2 - q_1)^2}{(u_2 + q_1)^2 + (u_1 - q_2)^2},$$

or

$$\left(\frac{1 - \cos i}{1 + \cos i} \right)^4 = \frac{(u_3 + q_4)^2 + (u_4 - q_3)^2}{(u_4 + q_3)^2 + (u_3 - q_4)^2}.$$

In the case of a circular orbit and distribution of the light scattering material symmetric to the orbital plane, the first-harmonics terms are negligibly small and only the second-harmonics terms can reliably be used for the determination of the orbital parameters. In addition to the orbital inclination, the orientation of the orbit on the sky (longitude of ascending node Ω) can be found from (Drissen et al. 1986) as follows:

$$\tan \Omega = \frac{A + B}{C + D} = \frac{C - D}{A - B}, \quad (4)$$

⁴ <https://docs.scipy.org/doc/scipy/reference/optimize.html>

⁵ <https://www.aavso.org/bob-nelsons-o-c-files>.

³ <https://gea.esac.esa.int/archive/>

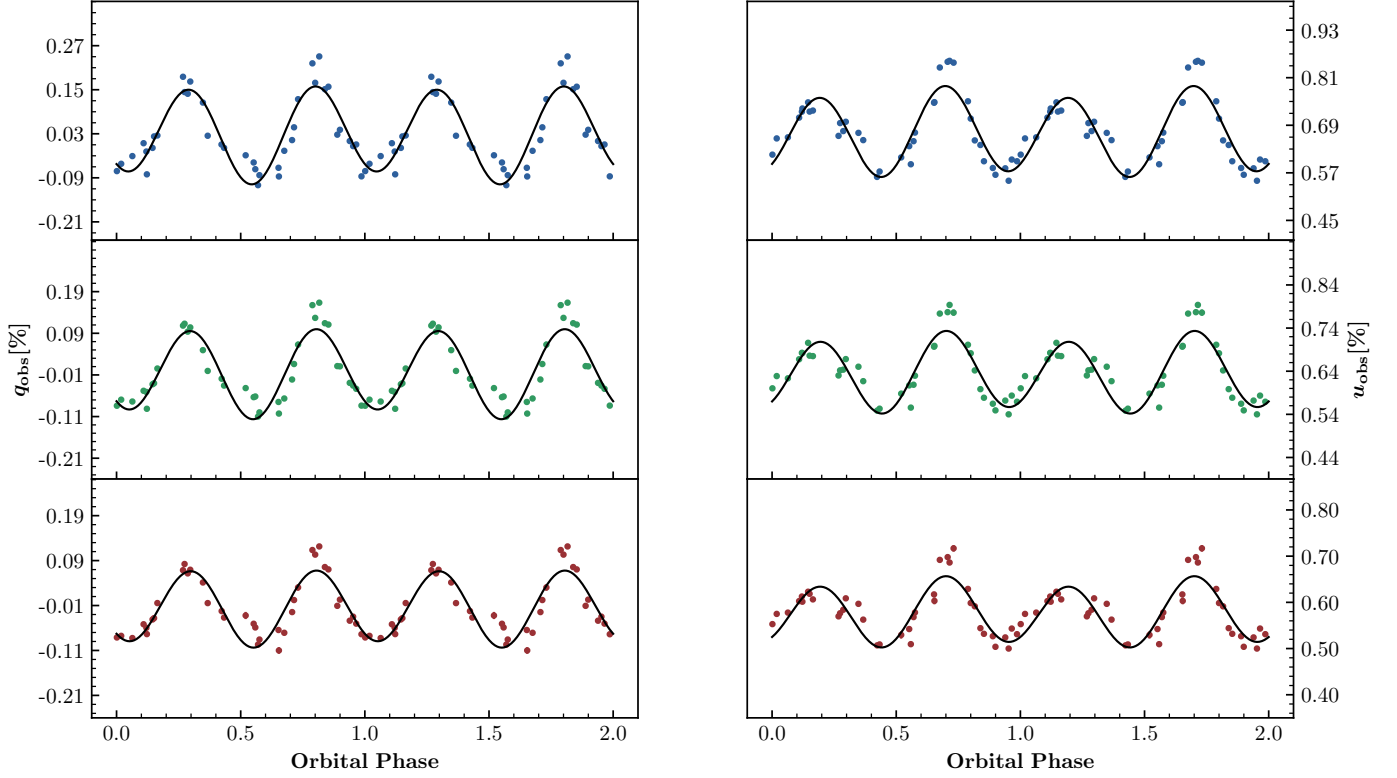


Fig. 4. Variability of observed Stokes q and u parameters for AO Cas in B , V , and R passbands shown in the top, middle, and bottom panels, respectively, which are phase-folded at the orbital period of 3.52 days. Fourier fit curves (see Sect. 3.3) are shown in solid lines and the best fit Fourier coefficients are given in Table 5. For the majority of data points, the length of $\pm\sigma$ error bars is shorter than the size of the plotting symbols.

Table 5. Best-fit Fourier coefficients for Stokes q and u .

Passband	q_0	q_1	q_2	q_3	q_4	u_0	u_1	u_2	u_3	u_4
B	0.0304	0.0181	0.0007	-0.1026	-0.0664	0.6694	0.0017	-0.0165	-0.0796	0.0662
	± 0.0067	± 0.0095	± 0.0094	± 0.0098	± 0.0090	± 0.0055	± 0.0079	± 0.0078	± 0.0081	± 0.0075
V	-0.0077	0.0118	0.0015	-0.0814	-0.0600	0.6387	0.0031	-0.0144	-0.0683	0.0515
	± 0.0053	± 0.0077	± 0.0075	± 0.0079	± 0.0073	± 0.0049	± 0.0070	± 0.0069	± 0.0073	± 0.0067
R	-0.0155	0.0069	0.0016	-0.0650	-0.0497	0.5736	0.0020	-0.0127	-0.0539	0.0420
	± 0.0042	± 0.0061	± 0.0058	± 0.0062	± 0.0056	± 0.0044	± 0.0063	± 0.0060	± 0.0064	± 0.0058

where,

$$\begin{aligned}
 A &= \frac{u_4 - q_3}{(1 - \cos i)^2}, & B &= \frac{u_4 + q_3}{(1 + \cos i)^2}, \\
 C &= \frac{q_4 - u_3}{(1 + \cos i)^2}, & D &= \frac{u_3 + q_4}{(1 - \cos i)^2}.
 \end{aligned} \quad (5)$$

Moreover, A_q , and A_u are two parameters which define the ratio of the amplitudes of second to first harmonics for Stokes q and u , respectively. For a circular orbit, these parameters are effective measures of the degree of symmetry and the concentration scattering material towards the orbital plane. Their values were obtained from the following formulae:

$$A_q = \sqrt{\frac{q_3^2 + q_4^2}{q_1^2 + q_2^2}}, \quad A_u = \sqrt{\frac{u_3^2 + u_4^2}{u_1^2 + u_2^2}}. \quad (6)$$

With Eqs. 3-6, we have derived the values of i , Ω , A_q , and A_u for the B , V , and R passbands, given in Table 6. As is seen from this table, second harmonics variations are clearly dominating in the polarization variability of AO Cas.

Figure 5 shows the ellipses of the second harmonics on the (q, u) plane, with the derived Stokes parameters of the IS polarization for the B , V , and R passbands. The eccentricity of the ellipses is related to the inclination of the orbit, i , and the orientation of their major semi-axes with respect to q -axis defines the orientation of the orbit, Ω . The direction of circumvention corresponds to the direction of the orbital motion in the binary system on the plane of the sky. In the case of AO Cas, this direction is clockwise.

In addition to the strong second harmonics, there is a small, but non-zero first harmonics in the variability of Stokes parameter, u , at the significance level of $\sim 2\sigma$. We note, that the presence of the first harmonics is also apparent in the data obtained by Rudy & Kemp (1976). Thus, the slight asymmetry of light scattering material with respect to the orbital plane in the AO Cas appears to be real.

Comparison of the B passband polarization variability curve of the Stokes parameters shown in our Figure 4, with that published by Rudy & Kemp (1976)⁶, reveals their remarkable

⁶ Note: the variability "curves" plotted by Rudy & Kemp (1976) for their measured Stokes parameters are hand-drawn.

Table 6. Orbital parameters of AO Cas in *B*, *V*, and *R* passbands.

Passband	i^a	Ω	A_q/A_u
<i>B</i>	63.67°	$30.39^\circ(210.39^\circ)$	6.75/6.25
<i>V</i>	63.22°	$29.82^\circ(209.82^\circ)$	8.63/10.11
<i>R</i>	62.34°	$27.16^\circ(207.16^\circ)$	10.94/9.29

Notes. ^(a) The values given are de-biased and are 2° lower than biased values.

similarity. Even the higher secondary peaks in Stokes q and u at the phase 0.75 are visible on the new and old plots, which are separated in time by half a century. In contrast to (Pfeiffer 1976), our polarization phase curves do not show evidence for long-term effects, such as seasonal changes. Our new results are strongly suggesting that general distribution of light scattering material in the AO Cas system remains stable over many decades. Therefore, the conclusion made by (Pfeiffer 1976) about noticeable cycle-to-cycle variability is most likely due to the low accuracy of his polarization data.

As is well known, due to the noise in polarimetric data arising from measurement uncertainties, the value of i derived from the Fourier fit is always biased towards higher values (Aspin et al. (1981); Simmons et al. (1982); Wolinski & Dolan (1994)). The amount of bias also depends on the value of true inclination, the lower the true value of i , the higher is the bias. A similar bias may be induced due to stochastic noise caused by intrinsic non-periodic component in polarization variations (Manset & Bastien 2000). Obviously, the deviations of the data from the fit can also be due to departure of the binary viewing geometry from the BME model assumptions, such as the absence of stellar eclipses and/or occultations of the light scattering regions occurring at certain range of the orbital phase.

As is seen from Table 6, the values of i and Ω derived for the three passbands are in good agreement with each other. There is an ambiguity on the value of Ω as $\Omega + 180^\circ$ is equally possible (Drissen et al. 1986). Because AO Cas is a (partially) eclipsing binary, the true value of inclination is rather high, and that should mean a smaller bias. In order to account for such bias, we derived confidence intervals for i and Ω defined by Wolinski & Dolan (1994). This method utilizes the special merit parameter γ , given as follows:

$$\gamma = \left(\frac{A}{\sigma_p} \right)^2 \frac{N}{2}, \quad (7)$$

where A is the fraction of the amplitude of polarization variability:

$$A = \frac{|q_{\max} - q_{\min}| + |u_{\max} - u_{\min}|}{4}, \quad (8)$$

and σ_p is a standard deviation that is determined from the scatter of the observed Stokes parameters around the best fit curves, N is the number of observations, and q_{\max} , q_{\min} , u_{\max} , u_{\min} are the maximum and minimum values of the fitted Stokes parameters q and u . The values of γ we derived for the *B*, *V*, and *R* passbands are 380, 345, and 320, respectively.

In order to estimate the bias and 1σ confidence intervals for i and Ω , we used the plots given in (Wolinski & Dolan (1994), Figs. 4 and 6 therein). The resulting de-biased values of i and Ω averaged over *B*, *V*, and *R* passbands are $63^\circ + 2^\circ / - 3^\circ$ and

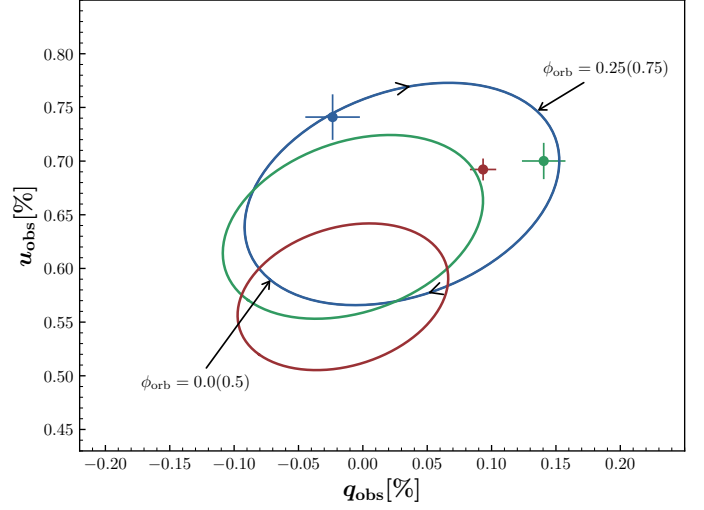


Fig. 5. Variability of observed polarization for AO Cas plotted on the Stokes (q , u) plane, represented by the ellipses of second harmonics of Fourier fit. The clockwise direction and phases of the orbital period are depicted on *B* passband ellipse. The angle between the major axis and the q -axis gives the orientation Ω . Average interstellar Stokes q and u parameters are depicted by circles with $\pm\sigma$ error bars. Blue, green, and red colors represent *B*, *V*, and *R* passbands.

$29^\circ(209^\circ) \pm 8^\circ$, respectively. Furthermore, we compared our derived value of i with the values given by other sources. Schneider & Leung (1978) obtained the value of 51.7° from the analysis of photometric data, Rudy & Kemp (1976) used polarimetry to estimate the value of i from 57° to 60° ; Pfeiffer (1976) also used polarization to estimate an inclination $\sim 55^\circ$ and Gies & Wiggs (1991) used spectroscopic observations to derive the value of $i = 61.1^\circ \pm 3^\circ$. The modeling of Palate et al. (2011) gave a value $i \sim 65.7^\circ$. Orbital inclination derived from our polarimetry falls somewhere in between of those derived by Gies & Wiggs (1991) and Palate et al. (2011), and it is in good agreement with both.

4. Conclusions

Our new polarimetric study of O-type binary star system AO Cas has re-affirmed the existence of an intrinsic linear polarization, which is variable with the phase of binary orbital period. A Lomb-Scargle algorithm clearly detected an orbital period signal in our high-precision polarimetric data with no other frequency present. The amplitude of this variability is $\sim 0.2\%$ and now we are able to ascertain that most of the polarization observed from AO Cas is of an interstellar nature. The small value of intrinsic polarization allowed us to rule out the presence of large circumstellar scattering envelope, as previously suggested by Pfeiffer (1976). Our new results indicate that light scattering material in AO Cas is confined into a relatively small region and doesn't form an extended envelope around the system.

From a comparison of our variability curve in the *B* passband with that obtained by Rudy & Kemp (1976), we have found that they are remarkably similar in amplitude and shape. This gives strong arguments in favor of a stable distribution of light scattering material in the AO Cas binary system. We have not found evidence of seasonal changes in the intrinsic polarization in AO Cas. Our new data have confirmed the presence of small (but not negligible) first-harmonics variations

in Stokes u parameter, pointing to some asymmetry in the distribution of scattering material in the binary system. From the two-harmonics Fourier fit to the observed variations in the Stokes parameters, the estimates for the inclination, $i = 63^\circ + 2^\circ / - 3^\circ$, and orientation of the orbit, $\Omega = 29^\circ(209^\circ) \pm 8^\circ$. The direction of motion on this orbit, as seen on the sky, is clockwise. The inclination of the orbit derived from polarimetry is in a good agreement with the latest determinations made with other methods.

We intend to continue our polarimetric studies of O-type binary star systems, originally initiated by Berdyugin et al. (2016), who discovered variable phase-locked polarization in HD 48099. We have observed another similar binary system, namely, DH Cephei. The initial data analysis shows phase-dependent polarization variability in DH Cep, just as in HD 48099 and AO Cas. In the near future, we will present the results of our numerical scattering code modeling for AO Cas and DH Cep systems. This modeling will certainly help in shedding more light on the distribution of light-scattering material in O-type binaries.

Acknowledgements. This work was supported by the ERC Advanced Grant Hot- Mol ERC-2011-AdG-291659 (www.hotmol.eu). Dipol-2 was built in the cooperation between the University of Turku, Finland, and the Kiepenheuer Institut für Sonnenphysik, Germany, with the support by the Leibniz Association grant SAW-2011-KIS-7. We are grateful to the Institute for Astronomy, University of Hawaii for the observing time allocated for us on the T60 telescope at the Haleakalā Observatory. All raw data and calibrations are available on request from the authors.

References

- Aspin, C. & Simmons, J. F. L. 1982, MNRAS, 199, 601
 Aspin, C., Simmons, J. F. L., & Brown, J. C. 1981, MNRAS, 194, 283
 Berdyugin, A., Piirola, V., Sadegi, S., et al. 2016, A&A, 591, A92
 Brown, J. C., McLean, I. S., & Emslie, A. G. 1978, A&A, 68, 415
 Drissen, L., Lamontagne, R., Moffat, A. F. J., Bastien, P., & Seguin, M. 1986, ApJ, 304, 188
 Gaia Collaboration, Brown, A. G. A., Vallenari, A., et al. 2021, A&A, 649, A1
 Gies, D. R. & Wiggs, M. S. 1991, ApJ, 375, 321
 Hutchings, J. B. & Hill, G. 1971, ApJ, 167, 137
 Kosenkov, I. A. & Veledina, A. 2018, MNRAS, 478, 4710
 Lomb, N. R. 1976, Ap&SS, 39, 447
 Manset, N. & Bastien, P. 2000, AJ, 120, 413
 Palate, M., Rauw, G., Gosset, E., & Nazé, Y. 2011, Bulletin de la Societe Royale des Sciences de Liege, 80, 504
 Pfeiffer, R. J. 1976, AJ, 81, 1000
 Pfeiffer, R. J. & Koch, R. H. 1973a, Information Bulletin on Variable Stars, 780, 1
 Pfeiffer, R. J. & Koch, R. H. 1973b, in Bulletin of the American Astronomical Society, Vol. 5, 345
 Pfeiffer, R. J. & Koch, R. H. 1976, in Bulletin of the American Astronomical Society, Vol. 8, 362
 Piirola, V., Berdyugin, A., & Berdyugina, S. 2014, in Society of Photo-Optical Instrumentation Engineers (SPIE) Conference Series, Vol. 9147, Ground-based and Airborne Instrumentation for Astronomy V, ed. S. K. Ramsay, I. S. McLean, & H. Takami, 91478I
 Piirola, V., Kosenkov, I. A., Berdyugin, A. V., Berdyugina, S. V., & Poutanen, J. 2021, AJ, 161, 20
 Plavec, M. 1970, PASP, 82, 957
 Price-Whelan, A., Sipocz, B., Daniel, Major, S., & Oh, S. 2018, Adm/Gala: V0.3
 Rudy, R. J. & Kemp, J. C. 1976, ApJ, 207, L125
 Rudy, R. J. & Kemp, J. C. 1978, ApJ, 221, 200
 Scargle, J. D. 1982, ApJ, 263, 835
 Schmidt, G. D., Elston, R., & Lupie, O. L. 1992, AJ, 104, 1563
 Schneider, D. P. & Leung, K. C. 1978, ApJ, 223, 202
 Shannon, C. 1949, Proceedings of the IRE, 37, 10
 Simmons, J. F. L., Aspin, C., & Brown, J. C. 1982, MNRAS, 198, 45
 Suveges, M. 2012, in Seventh Conference on Astronomical Data Analysis, ed. J.-L. Starck & C. Surace, 16
 VanderPlas, J. T. 2018, ApJS, 236, 16
 Wolinski, K. G. & Dolan, J. F. 1994, MNRAS, 267, 5

Appendix A: Log of polarimetric observations**Table A.1.** Log of polarimetric observations for AO Cas.

Date	MJD	T_{exp} [s]	N_{obs}
2020-10-26	59148.97	240	80
2020-10-31	59153.89	240	80
2020-11-01	59154.87	240	80
2020-11-03	59156.88	240	80
2020-11-04	59157.86	243	81
2020-11-05	59158.89	150	50
2020-11-08	59161.84	240	80
2020-11-09	59162.90	216	72
2020-11-10	59163.84	240	80
2020-11-13	59166.82	240	80
2020-11-14	59167.88	240	80
2020-11-16	59169.82	240	80
2020-11-17	59170.85	240	80
2020-11-19	59172.81	240	80
2020-11-20	59173.82	240	80
2020-11-26	59179.81	135	45
2020-11-27	59180.82	240	80
2020-11-30	59183.81	240	80
2020-12-01	59184.78	240	80
2020-12-02	59185.78	144	48
2020-12-25	59208.83	240	80
2020-12-26	59209.80	240	80
2020-12-28	59211.80	240	80
2020-12-29	59212.81	240	80
2021-01-02	59216.80	240	80
2021-01-03	59217.79	240	80
2021-01-05	59219.80	240	80
2021-01-06	59220.80	240	80
2021-01-07	59221.80	240	80
2021-01-11	59225.81	240	80
2021-01-12	59226.79	240	80
2021-01-13	59227.80	240	80
2021-01-14	59228.81	240	80
2021-01-15	59229.79	240	80
2021-01-16	59230.79	240	80
2021-01-28	59242.76	240	80
2021-01-29	59243.75	240	80
2021-01-31	59245.75	240	80
2021-02-01	59246.75	240	80